An Additive Model as a Physical Basis for Shadow Fading

Jari Salo, Lasse Vuokko, Hassan M. El-Sallabi and Pertti Vainikainen

Abstract

Received signal power in mobile wireless communications is typically modelled as a product of three factors: distance-dependent average path loss law, variation in the local mean power (shadow fading), and small-scale fading. Of these three factors, the least investigated is the shadow fading, which is usually explained as a result of *multiplication* of large number of random attenuating factors in the radio channel. In this paper we propose an *additive* model as an alternative physical basis for shadow fading within an area where path loss is constant. Starting from a sum-of-sinusoids signal model, we show that under mild statistical assumptions on the powers of the sinusoids, the resulting signal power will have approximately Gaussian distribution in logarithmic scale. A cluster-based model for shadow fading emerges as a special instance of the general result. We present simulation and measurement results that support our theoretical findings. The new physical basis for shadow fading also provides insights into simulation and modelling of radio channels.

Index Terms

Lognormal distribution, shadow fading, channel modelling, central limit theorem, channel measurements, multipath clusters.

This work was supported by the Academy of Finland, Nokia Foundation, Foundation of Commercial and Technical Sciences, TKK Foundation, and Graduate School of Electronics, Telecommunications, and Automation. The authors are with the SMARAD Centre of Excellence, Radio Laboratory, Helsinki University of Technology, P.O. Box 3000, FI-02015-TKK, Finland (e-mail: jari.salo@tkk.fi; lasse.vuokko@tkk.fi; hsallabi@cc.hut.fi; pertti.vainikainen@tkk.fi). Part of this paper has been presented at IEEE VTC-spring'06, Melbourne, May 2006.

I. INTRODUCTION

It is common practice in radio communications that amplitude variation of a received radio signal is modelled as a product of path loss, shadow fading and small-scale fading [1]. Several models exist for path loss, including the variants of Okumura-Hata and Walfisch-Ikegami formulas. Likewise, numerous statistical models have been proposed for small-scale fading, most notably the Rayleigh, Rice and Nagakami-m probability laws. Shadow fading, apparently first reported in [2], has been empirically observed to obey approximately lognormal distribution in a wide variety of propagation environments, yet few theories for the lognormality have been presented. This is somewhat startling since, from mobile communications system point of view, shadow fading plays a key role in interference modelling as well as in the analysis of handover algorithms, slow power control, macrodiversity and network planning tools and simulation.

The conventional textbook explanation for the lognormality of shadow fading is the *multiplicative* model which assumes that there are several random multiplicative factors attenuating the received signal, and the logarithm of their product approaches the Gaussian distribution for a sufficiently large number of such factors. This hypothesis has some shortcomings, however. First of all, it has been shown in [3] that convergence of the sum-of-logs to a Gaussian random variable requires a large number of multiplicative factors, e.g. a cascade of more than 30 independent Rayleigh distributed attenuations (see also [4]). Urban microcell and macrocell measurements indicate that the number of interactions (reflections, diffractions) experienced by the dominant propagation paths is typically much smaller than this, e.g. less than five in small urban macro cells [5], [6]. Second, it was remarked in [7] that, should the multiplicative shadow fading model be correct, the path loss itself should increase exponentially with distance. This disagrees with empirical evidence, which suggests a $\sim d^m$ path loss law with distance d. The path loss exponent m is typically found in the range $3...5$, depending on the environment. Third, we point out that, under the multiplicative model, there should exist systematic experimental evidence of an increase in the shadow fading standard deviation with distance, since the number of random multiplicative attenuations is expected to increase, on average, as the distance between receiver and the transmitter increases. However, most measurement studies indicate that the standard deviation is approximately distance independent. While these observations do not rule out the multiplicative model, it is nevertheless clear that the classical ‘textbook theory’ for shadow fading does not fully agree with the measurement results currently available in literature. For this reason as well as for mathematical tractability, other distributions have also been proposed to model shadow fading, including the gamma distribution [8]. Without a physical basis, however, it is difficult to justify using one arbitrary probability model over another. Therefore, it is important to investigate the underlying physical process in order to find theoretically justified probability models.

Some studies to explain the lognormality of shadow fading have appeared in literature. In [9] it was shown that in urban environment lognormal variation in mean path loss may be caused by randomness in building heights. Somewhat contradictively, [10] reports that not only random rooftop heights are sufficient to produce lognormal local area power, but also randomized building construction and effect of foliage would be required. The results in [9], [10] focus on the global shadow fading, to be defined later in the paper. Therefore, they cannot explain the observed variations in local mean within a smaller area, where path loss is constant. A groundbreaking hypothesis was presented in [7], [11], where it was argued that time-variant multiple scattering in the propagation channel can cause the signal level variations usually perceived as lognormal. Interestingly, measurement-based evidence to support the theory in forest and urban propagation scenarios was also presented. In [12], it was shown that in a line-of-sight microcell few dominant reflections lead to slow variations in the signal power that can be modelled using Nagakami-m or lognormal distribution. Unfortunately, the results therein were not generalized to other environments, nor were any analytical justifications given. This is exactly the novelty and main contribution of the present paper. We present an *additive* sum-of-sinusoids based model to explain shadow fading of a narrowband radio signal, and provide a simple analytical justification for its lognormality. As a special case of the general sum-of-sinusoid model, we also present a cluster-based model, that is easier to verify with measurements than the general model. Our analysis is focused on a geographical area within which path loss is constant, and therefore differs from [9], [10], that consider the effect of random path loss parameters in a larger (global) area. Motivated by the theoretical findings and literature review, we define the concepts of local and global shadow fading, and discuss their role in channel modelling and simulation.

The paper is organized as follows. In Section II we present the main result of the paper, a sum-of-sinusoids based explanation for local shadow fading. Section III describes a simplified cluster-based model. Simulation examples and measurement results are given in Section IV. In Section V we compare our results to literature and discuss their implications for channel modelling. Section VI concludes the paper.

Notation: We denote a random variable and its realization with $\mathcal{X}$ and x, respectively. The expected value and variance of $\mathcal{X}$ are denoted with $E[\mathcal{X}]$ and $\mathrm{var}[\mathcal{X}]$. A vector in three-dimensional space is denoted $\vec{z}$, and a scalar with z. A set $\{X_1, X_2, \ldots, X_N\}$ is also denoted with $\{X_n\}_{n=1}^N$, or just $\{X_n\}$ when N is obvious from the context.

II. An Explanation of Shadow Fading Based on the Sum-Of-Sinusoids Model

In this section we present our main result: an additive sum-of-sinusoid based model as a basis for shadow fading.

A. Main Result

Here we present the main result, deferring the details of proof to Section II-B. We begin by defining *local area* and *extended local area*. Essentially, the difference between the two is that within a local area only small-scale fading takes place, while within the extended local area also shadow fading occurs.

Definition 1: Local area (LA) is defined as the largest volume of free space, where the received narrow-band signal can be written as a superposition of N homogeneous plane waves [13]:

$$h(\vec{x}) = \sum_{n=1}^{N} a_n e^{j(\vec{k}_n \cdot \vec{x} + \theta_n)}\,, \tag{1}$$

where a_n is a constant positive amplitude, and $\vec{k}_n \cdot \vec{x}$ is the dot product of the nth three-dimensional wave vector $\vec{k}_n$ and position vector $\vec{x}$. The parameter θ_n is the phase of the nth plane wave in $\vec{x} = \vec{0}$, i.e., the origin of the coordinate system. We assume that parameters $\{a_n\}_{n=1}^N$, $\{\vec{k}_n\}_{n=1}^N$, $\{\theta_n\}_{n=1}^N$, and N are constants within a local area. Further, it is assumed that $\vec{k}_m \neq \vec{k}_n$ for all

$m \neq n$, or, equivalently, that all plane waves have different arrival angles; this assumption is sometimes called heterogeneous scattering [13].

The effect of antenna on the nth plane wave is included in a_n and θ_n. [In this paper, we use the terms plane wave, ray, and sinusoid interchangeably to refer to a single term in the sum (1)].

As the receiver moves within the local area, small-scale fading results due to change in the position vector $\vec{x}$. The signal power averaged over the local area is approximately

$$P_N \approx \sum_{n=1}^{N} a_n^2 \,. \tag{2}$$

The approximation (2) will be justified in Section II-B. Interestingly, in [14] the sum of plane wave powers $\sum_{n=1}^{N} a_n^2$ is called the 'shadowing term'.

As the receiver moves outside the local area, the powers of the plane waves, and hence P_N, cannot be anymore assumed constant. The variation in the plane wave powers can be thought to be caused by slow changes in the scattering cross-section of the last-bounce interacting object as seen by the receiver. There may also be other causes, such as a short-term obstruction by lamp posts, cars, etc. In this paper we are not concerned with the underlying physics of the power variation mechanism. Instead we model the plane wave powers as random processes, and examine the distribution of the received power within a larger volume, called an extended local area.

Definition 2: The *extended local area* (ELA) is defined as the largest volume in which the plane wave powers $\{\mathcal{A}_n^2\}_{n=1}^{N}$ can be characterized as stationary random variables[1], and N is a constant.

By spatial sampling of the extended local area we can then regard the sequence of local area powers, say $\{P_{N,1}, P_{N,2}, \ldots\}$, as realizations of a random variable $\mathcal{P}_N = \sum_{n=1}^{N} \mathcal{A}_n^2$. Due to assumptions of stationarity and fixed N, the mean power in the extended local area, i.e., $E[\mathcal{P}_N]$, will be constant, which further implies that the path loss is constant within the extended local area. We stress that here we mean the true path loss, and not the path loss given by any path

[1] We remind the reader that $\mathcal{A}_n$ denotes a random variable, while a_n denotes its realization.

loss model; therefore the following development does not depend on a path loss model of any kind. For an illustration of the definitions of local area and extended local area, see Fig. 1.

The main result of the paper is the following. The proof is given in Section II-B.

Result 1: Assume that the random variables $\{\mathcal{A}_n^2\}_{n=1}^N$ are independent, and that for all n it holds that

$$\lim_{N\to\infty} \frac{E[(\mathcal{A}_n^2 - \mu_N)^3]}{\sigma_N^3} = 0\,, \tag{3}$$

where $\mu_N = E[\mathcal{P}_N]$, and $\sigma_N^2 = \mathrm{var}[\mathcal{P}_N]$. Then, as $N \to \infty$, the random variable $\ln\left(\frac{\mathcal{P}_N}{\mu_N}\right)$ converges in distribution to a Gaussian random variable with zero mean and variance σ_N^2.

Result 1 states that $\ln(\mathcal{P}_N)$ is approximately Gaussianly distributed if N is large. The practical significance of the result lies in the fact that the lognormality of shadow fading observed in numerous measurements can also arise from an *additive* model, instead of a multiplicative one. Hence, the result provides an alternative physical basis for shadow fading. Note that in Result 1 it is *not* required that $\{\mathcal{A}_n^2\}_{n=1}^N$ are identically distributed.

Remark 1: In Result 1, the normalization by μ_N is needed to keep the mean of $\ln\left(\frac{\mathcal{P}_N}{\mu_N}\right) = -\ln(\mu_N)+\ln(\mathcal{P}_N)$ finite in the limit $N \to \infty$. In a practical interpretation of Result 1, the number of plane waves, N, is finite and the normalization can be dropped. Indeed, the normalization term $-\ln(\mu_N)$ is a deterministic constant (for fixed N), that only shifts the mean of the distribution of $\ln(\mathcal{P}_N)$, but does not affect its shape or variance, i.e., $\mathrm{var}\left[\ln(\frac{\mathcal{P}_N}{\mu_N})\right] = \mathrm{var}\left[\ln(\mathcal{P}_N)\right]$. In measurement analysis of shadow fading one typically normalizes the mean value of the measured power data record to 0 dB. As we are primarily interested in explaining the experimentally observed Gaussian shape (in dB) of the shadow fading distribution, we can, for all practical purposes, drop the 'technical' scaling factor $-\ln(\mu_N)$.

Remark 2: Stated in decibels, Result 1 says that the variance of the random variable $10\log_{10}(\mathcal{P}_N)$ is $(\frac{10}{\ln(10)})^2\,\mathrm{var}[\ln(\mathcal{P}_N)] \approx 18.86\,\mathrm{var}[\ln(\mathcal{P}_N)]$.

Remark 3: In this paper we focus on the distribution of $\ln(\mathcal{P}_N)$ within an extended local area. We consider spatial correlation properties of shadow fading beyond scope, and consequently do not make any unnecessary assumptions of the direction of movement or velocity of the receiver.

In Fig. 2 we illustrate the theory for $N = 100$ lognormally distributed rays. Lognormal distribution has been proposed in literature as the shadow fading distribution for individual delay bins in both outdoor [15] and indoor measurements [16] with the number of plane waves reported ranging from about a dozen to several hundreds [15]–[20]. We consider two cases: iid lognormal shadow fading distributions for all rays, and unequal powers with a decay rate $-0.4n$ dB, $n = 0, \ldots, N-1$, for the nth ray, with respect to the first ray. The latter case corresponds to the case with exponential power decay with rms delay spread of $0.2\ \mu s$, assuming that the 100 rays arrive with uniformly spaced delays. In Fig. 2 the x-axis of the histogram shows shadow fading in decibels, i.e., $10\log_{10}(\mathcal{P}_N)$. We note that, by visual inspection, the distributions are quite similar to a Gaussian one. Slight skewness remains since the convergence of a sum of lognormal variates to the Gaussian distribution is quite slow if the standard deviation of the component distributions is large. Depending on the distributions of the plane wave powers, their number N need not necessarily be large for Result 1 to hold (e.g. $N = 4$ can be sufficient) as we shall illustrate later in Section IV.

B. Proof of the Main Result

We first justify (2). Received power averaged spatially over the local area is given by [13]

$$P_N = \frac{1}{|V|} \int_V |h(\vec{x})|^2 d\vec{x}\,, \tag{4}$$

where the integration is over the volume V of the local area, and $|V|$ denotes the total volume of the local area. The power of the complex envelope is

$$|h(\vec{x})|^2 = \sum_{n=1}^{N} a_n^2 + \sum_{k\neq l} a_k a_l e^{j(\theta_k - \theta_l)} e^{j(\vec{k}_k - \vec{k}_l)\cdot\vec{x}} \tag{5}$$

In [14], the first term of (5) is interpreted as shadowing, while the latter term is identified as the source of small-scale fading and “medium-term variation”. It is well known [13] that if $\vec{k}_m \neq \vec{k}_n$ for all $m \neq n$, then $\lim_{|V|\to\infty} P_N = \sum_{n=1}^{N} a_n^2$. For a finite-volume cube-shaped local area we can write (4) as

$$P_N = \sum_{n=1}^{N} a_n^2 + \underbrace{\sum_{k \neq l} a_k a_l e^{j(\theta_k - \theta_l)} \frac{1}{L^3} \int_{-\frac{L}{2}}^{\frac{L}{2}} \int_{-\frac{L}{2}}^{\frac{L}{2}} \int_{-\frac{L}{2}}^{\frac{L}{2}} e^{j(\vec{k}_k - \vec{k}_l) \cdot \vec{x}} \, \mathrm{d}x \, \mathrm{d}y \, \mathrm{d}z}_{\epsilon}$$

where ϵ is the approximation error due to finite $|V| = L^3$. This error can be expressed as, with $\operatorname{sinc}(x) = \sin x / x$,

$$\begin{aligned} \epsilon &= \sum_{k \neq l} a_k a_l e^{j(\theta_k - \theta_l)} \operatorname{sinc}\left(\frac{c_{kl,x} L}{\lambda}\right) \operatorname{sinc}\left(\frac{c_{kl,y} L}{\lambda}\right) \operatorname{sinc}\left(\frac{c_{kl,z} L}{\lambda}\right) && (6) \\ &\leq \frac{\lambda^3}{L^3} \sum_{k \neq l} \frac{a_k a_l e^{j(\theta_k - \theta_l)}}{c_{kl,x} c_{kl,y} c_{kl,z}} && (7) \\ &= O(L^{-3}), \quad L \to \infty \,. && (8) \end{aligned}$$

In (6), λ is the wavelength, $c_{kl,q} = (\vec{u}_k - \vec{u}_l) \cdot \vec{e}_q$, $q = \{x, y, z\}$, $\vec{u}_n$ is the unit wavevector of the nth plane wave, and $\vec{e}_q$ is a unit basis vector of the cartesian coordinate system. In (7) we have used $\operatorname{sinc} x \leq 1/x$, and assumed[2] that $c_{kl,q} \neq 0$ for all $k \neq l$ and all $q = \{x, y, z\}$. Note that (7) implies that the size of the local area can be normalized by wavelength.

The result (8) essentially says that the error in the approximation $P_N \approx \sum_{n=1}^{N} a_n^2$ decreases inversely with respect to the volume of the local area. The error term ϵ may be significant if the local area is small and some of the plane waves' angles of arrival are closely spaced. Such a case gives rise to multipath interference varying slowly with distance, and can, in fact, be interpreted as another shadow fading mechanism. In principle, the largest volume of the local area is limited to a fraction of the distance to the nearest last-bounce interacting object, since as the receiver moves its scatter cross-section (and hence plane wave amplitude) will change faster than that of a faraway last-bounce object. See also [13, p. 84] for a discussion on local area size. In this paper, however, we focus on the modelling of $\sum_{n=1}^{N} a_n^2$ and assume that the volume of the local area is large enough, so that $\epsilon \ll \sum_{n=1}^{N} a_n^2$, or, equivalently, that (2) holds

[2]This assumption is made for convenience only and can be relaxed. For a pathological choice of the wavevectors $\{\vec{u}_n\}_{n=1}^{N}$, the worst-case convergence, under the heterogeneous scattering assumption, can be $\epsilon = O(L^{-1})$, $L \to \infty$. This happens if the angular difference vector $\vec{u}_k - \vec{u}_l = \vec{e}_q$ for some k, l, q.

with good accuracy. In reality, this is only an approximation that can nevertheless be justified in many outdoor propagation scenarios.

For a given local area within the extended local area, a_n^2 is a realization of a random variable $\mathcal{A}_n^2$. It is evident that the distribution of $\mathcal{P}_N = \sum_{n=1}^{N} \mathcal{A}_n^2$ will converge to Gaussian as N increases. To formalize this statement, we invoke the well-known Lyapunov's version of the central limit theorem, reproduced here for convenience. For a proof, see e.g. [21, p. 362]

Theorem 1: (Central Limit Theorem) Assume that $\{\mathcal{A}_n^2\}_{n=1}^{N}$ are independent random variables with means $\{\mu_n\}_{n=1}^{N}$, variances $\{\sigma_n^2\}_{n=1}^{N}$, and distributions $\{F_n\}_{n=1}^{N}$. Denote $\bar{\mu}_N = N^{-1}\sum_{n=1}^{N}\mu_n$, $\bar{\sigma}_N^2 = N^{-1}\sum_{n=1}^{N}\sigma_n^2$, and suppose that $\lim_{N\to\infty}\bar{\sigma}_N^2 < \infty$. Assuming that, for all n and some $\delta > 0$, it holds that

$$\lim_{N\to\infty} \frac{E[(\mathcal{A}_n^2 - N\bar{\mu}_N)^{2+\delta}]}{(\sqrt{N}\bar{\sigma}_N)^{2+\delta}} = 0\,, \tag{9}$$

then, as $N \to \infty$, the partial sums

$$\frac{\mathcal{P}_N - N\bar{\mu}_N}{\sqrt{N}\bar{\sigma}_N}$$

converge to a random variable with Gaussian distribution with zero-mean and unit variance.

By Theorem 1, the distribution of local area power $\mathcal{P}_N$, sampled over an extended local area, can be approximated with a Gaussian random variable with mean $\mu_N = N\bar{\mu}_N$ and variance $\sigma_N^2 = N\bar{\sigma}_N^2$. Result 1 states that also $\ln(\mathcal{P}_N)$ will be asymptotically (in N) Gaussian. The proof is based on the following theorem from [22, Th. 3.1.A]. In Theorem 2 by 'asymptotically Gaussian' we mean that the random variable $\mathcal{X}_m$ converges 'in distribution' to a Gaussian random variable as m tends to infinity [22].

Theorem 2: Suppose that $\mathcal{X}_1, \mathcal{X}_2, \ldots, \mathcal{X}_m$ are asymptotically Gaussian random variables with mean $E[\mathcal{X}_m] = \mu$, and variance $\sigma_m^2 = \mathrm{var}[\mathcal{X}_m]$, such that $\lim_{m\to\infty}\sigma_m^2 = 0$. Let $g(x)$ be a continuously differentiable function with $g'(\mu) \neq 0$. Then, as $m \to \infty$, the random variable $g(\mathcal{X}_m)$ is asymptotically Gaussian with mean $g(\mu)$ and variance $\sigma_m^2[g'(\mu)]^2$.

The simple intuition behind Theorem 2 is that for a small enough variance (large m), the probability mass of $\mathcal{X}_m$ is concentrated in the neighborhood of its mean value, where a linear approximation for $g(x)$ is valid. Since a linear transformation of a Gaussian variable results in another Gaussian random variable, the theorem follows.

Proof: *(Result 1)* By assumption (3) in Theorem 1, condition (9) is fulfilled with $\delta = 1$. From the independence of $\{\mathcal{A}_n^2\}_{n=1}^N$ it then follows that the random variable $\mu_N^{-1}\mathcal{P}_N$ will be asymptotically Gaussian with unit mean and variance

$$\text{var}\left[\frac{\mathcal{P}_N}{\mu_N}\right] = \frac{\bar{\sigma}_N^2}{N\bar{\mu}_N^2} \,,$$

that vanishes as $N \to \infty$, since $\lim_{N\to\infty} \bar{\sigma}_N^2$ is finite by assumption. (Recall that $\mu_N = N\bar{\mu}_N$ and $\sigma_N^2 = N\bar{\sigma}_N^2$.) Applying Theorem 2 to the sequence $\{\mathcal{P}_1, \mathcal{P}_2, \ldots\}$ and $g(x) = \ln(x)$, Result 1 follows. ■

Remark 4: Although assumed here for simplicity, the requirement that $\{\mathcal{A}_n^2\}_{n=1}^N$ are statistically independent is not mandatory as there also exist central limit theorems for dependent random variables [21]–[23]. Therefore, $\mathcal{P}_N$ can be approximated with a Gaussian random variable under very mild conditions on the statistics of $\{\mathcal{A}_n^2\}$. Furthermore, as seen from Theorem 1, the assumption that third central moments of $\{\mathcal{A}_n^2\}$ are finite can be replaced with a less restrictive one that $E[(\mathcal{A}_n^2 - \mu_N)^{2+\delta}] < \infty$ for all n and some positive δ.

C. A Special Case

The conventional multiplicative shadow fading model can be considered a special case of the additive model presented in this paper. To see this, we can once again invoke the central limit theorem. *Within* the local area, where $\{a_n\}_{n=1}^N$ are deterministic constants, the real and imaginary parts of the small-scale fading signal will have zero-mean Gaussian distributions with variance $\frac{P_N}{2}$, i.e., local area power is P_N assuming that the real and imaginary parts are statistically independent. This means that signal amplitude within local area can be written as

$$|h(\vec{x})| = \sqrt{P_N}\, r(\vec{x}) = \sqrt{\sum_{n=1}^{N} a_n^2\, r(\vec{x})} \,, \tag{10}$$

where $r(\vec{x})$ is a Rayleigh random variable with $E[r(\vec{x})^2] = 1$. The form in (10) is the classical multiplicative textbook model for the shadow fading process, since when the receiver moves over the extended local area the power factor P_N is a random variable with approximately lognormal distribution, as shown in Result 1. In this sense, the results in this paper do not contradict the conventional modelling approach, where a shadow fading process multiplies the small-scale fading.

III. A Cluster-Based Shadow Fading Model

Although the explanation of shadow fading based on the sum-of-sinusoids signal model (1) is very general in nature, its unfortunate drawback is that it is difficult to verify by measurements with the current measurement technology. Even UWB measurements with a delay resolution of $100 - 200$ picoseconds cannot fully resolve all incident plane waves [18]. Furthermore, the measurement of time evolution of ray amplitudes presents double difficulty, since not only is it enough that the receiver is able to resolve all the incident rays in delay or wavevector (i.e., angle of arrival) domain, but it should be able to do so while the receiver is moving over the extended local area. Hence, verifying the general model from Section II by direct measurement of plane wave powers seems impractical.

An indirect approach can be devised by making use of the well-established fact, that multipath components tend to appear in clusters [24]–[28]. In Fig. 3 we show received signals from two clusters extracted from a channel measurement to be discussed in more detail in Section IV. It can be seen that the cluster signals exhibit fading in small and large distance scales. It is therefore conceivable that not only the composite signal – i.e., complex sum of signals from all clusters – but also individual clusters[3] show large-scale power trends, which could be called shadow fading. Motivated by this observation, we can group the N plane waves in (1) into K clusters. Assuming that the heterogeneous scattering assumption holds, the spatial averaging operation from (4) still applies and the received power, averaged over a local area, is

[3]Since clusters are typically identified visually from measurement data, a cluster is usually subjectively defined as a set of multipath components with 'similar' delays and arrival angles. The observed fading characteristics of a cluster will naturally depend on the spatial-temporal resolution of the measurement equipment and processing methods used.

$$
\begin{aligned}
P_K &= \sum_{k=1}^{K} \underbrace{\sum_{n \in \Omega_k} a_n^2}_{w_k^2} \\
&= \sum_{k=1}^{K} w_k^2 \,,
\end{aligned}
\tag{11}
$$

where Ω_k is a set of plane wave indices for the kth cluster. The index sets $\{\Omega_k\}_{k=1}^{K}$ are disjoint, so that each plane wave belongs to one cluster only. The power of the kth cluster within the local area is denoted by w_k^2. Again, it is assumed that the local area power $P_K = \sum_{k=1}^{K} w_k^2$ is a realization of a random variable $\mathcal{P}_K = \sum_{k=1}^{K} \mathcal{W}_k^2$ that is assumed stationary within the extended local area. In the present paper we are not concerned with the physical process underlying the cluster shadow fading; the power variation of individual clusters is described probabilistically and may be caused by any process satisfying the statistical assumptions in Result 1. Note that (2) and (11) are in mathematically equivalent forms, and in Result 1 one needs only to replace $\mathcal{A}_n$ with $\mathcal{W}_k$, and N with K to justify the approximate Gaussianity of $\ln(\mathcal{P}_K)$.

In Section IV we present novel measurement results on cluster shadow fading, which also allow us to test with measurements the cluster-based formulation in (11).

The clustered multipath approach forms also the basis for a number of geometric stochastic channel models, in which each cluster has its own random angular, delay, and fading characteristics [25], [29], [30]. In addition to being easier to verify by measurements, the model in (11) together with Result 1 provides a more realistic way for generation of shadow fading in channel simulators based on the clustering approach. More discussion will follow in Section V.

IV. Verification of the Model Based on Simulations and Measurement

In the previous sections we have presented an additive model as a physical explanation for shadow fading and its lognormality. In this section we first present some simulation examples, and then compare the simple cluster-based model to novel measurement results.

A. Simulation Examples

1) Sum-Of-Sinusoids Model: We illustrate the theory for the general sum-of-sinusoids model (1) by assigning different distributions to the plane wave powers $\{\mathcal{A}_n^2\}_{n=1}^N$, namely, lognormal, Weibull and gamma distributions. As a disclaimer, we are not arguing that any of these distributions would correspond to the 'true' probability law of $\{\mathcal{A}_n^2\}$, as such law may not exist in the first place. These distributions were selected merely to illustrate that approximate lognormality of shadow fading can result from almost *any* distributions of the plane wave powers. As already mentioned, measurement of time-variant plane-wave powers presents mammothian practical problems. It is therefore comforting to know that the behavior of individual rays has minimal effect on the probability law governing the behavior of the logarithm of their sum.

Results in Fig. 4, given for $N = 10$ and $N = 100$, show that already summation of 10 plane waves results in a Gaussian-like distribution in log domain. Increasing N makes the Gaussian fit better, as is to be expected. We remind the reader that, although assumed here for convenience of presentation, the distribution of the plane wave powers need not be identically distributed.

2) Cluster-Based Model: A similar test can be repeated for the simplified model based on cluster shadow fading from Section III. In Fig. 5 we show an example of four different cluster power distributions. In all cases, it is assumed that the number of clusters is four and all clusters have iid power pdfs. Histograms and best-fit Gaussian pdfs are shown for chi-squared, Weibull, gamma, and lognormally distributed cluster powers. It can be seen that, with the possible exception of the gamma pdf with its chosen parameters, the resulting shadow fading distribution is close to the Gaussian pdf. Again, we do *not* wish to argue that real-world cluster powers would follow any one of the pdfs used here; our purpose is merely to illustrate that the apparent lognormality of shadow fading can result from almost *any* cluster power distribution. Interestingly, sum of lognormal cluster powers gives a particularly good fit. It is important to note, however, that this is because a sum of few lognormal variates can be well approximated as lognormal [31], not because of Result 1. This point is further illustrated in the following goodness-of-fit test.

3) Goodness-of-fit test: In Fig. 6, we show Monte Carlo simulation results of the Kolmogorov-Smirnov goodness-of-fit test [32]. The test compares the distribution of $10\log_{10}(\mathcal{P}_N)$ to Gaussian distribution. The results shown are based on the Lilliefors modification of the K-S test where the mean and variance of the Gaussian distribution are estimated from data. For a given value of N, the test statistic was averaged over 30 trials with 10^4 iid samples in each trial. The test statistics was computed for several values of N. The critical value at 5% significance level is 0.0089; below this value the hypothesis that the data sample was generated from a Gaussian distribution is accepted in the K-S sense. A similar test was used in [3] to compare convergence speed of products and sums of random variables to various fading distributions. Some remarks of the test results follow.

- As predicted by Result 1, the distribution of $10\log_{10}(\mathcal{P}_N)$ becomes more Gaussian as the number of plane waves, N, increases. The convergence speed depends on the distributions of the plane wave powers, $\{\mathcal{A}_n^2\}_{n=1}^N$.
- To reach the critical value at 5% significance level, the number of plane waves for Weibull, χ_2^2 and gamma distributions is about 40, 130, and 800, respectively. For lognormal distributed ray power with standard deviation of 8 dB, the convergence is very slow, whereas for standard deviation of 4 dB, about 300 hundred plane waves need to be summed.
- Sum of lognormal variates gives a good fit both when N is small or N is large. The fit may be bad between these two extremes. Good fit for large N follows from Result 1, whereas for small N it follows from the fact that the distribution of a sum of lognormal random variables is approximately lognormal [31].
- Comparing Fig. 6 to Fig. 4 and Fig. 5, we note that even if the K-S test statistic is above the critical value, the distribution still resembles Gaussian by visual inspection. For example, the test statistic for 10 gamma distributed ray powers is about 0.05, and yet the corresponding distribution shown in the bottom row of Fig. 4 agrees with the best-fit Gaussian reasonably well. Similar conclusions apply to the other distributions shown in Figs. 4 and 5. The high value of the test statistic is in most cases caused by the non-Gaussian tails which do not fit the Gaussian distribution well.
- In shadow fading measurement literature, model fit is hardly ever confirmed with statistical goodness-of-fit tests because real-world measurement data often does not fit the tails of the Gaussian distribution. Further comments on this issue are made in Section V-B.

B. Measurement Results

Measurement results on the cluster shadow fading distributions appear not to be available in literature, probably due to many practical difficulties in both measurements and data processing (e.g. cluster extraction and tracking from measurement data over long measurement distances). In what follows, we present novel measurement results on cluster shadow fading distributions based on an earlier study in [5]. Measurements have been summarized in Table I. More detailed information on the measurements and the environment can be found in [5]. The measurement system and the channel estimation method are described in [33].

A total of ten clusters were identified from measurement data by visual inspection, as explained in [5]. The local area power of each cluster was estimated using sliding mean[4] with window width of 40 wavelengths (six meters). With most clusters, a slight residual power trend remained in the local mean signal, see Fig. 3 for an example. Hence the measurement route is too long to have constant path loss, and therefore does not strictly speaking fulfill the assumptions of extended local area. As a practical solution, the path loss trend was removed using a piecewise linear fit with a breakpoint distance of 500 wavelengths (75 meters).

Fig. 7 shows the histograms of zero-meaned local area powers of the cluster. Three strongest clusters carry more than 75% of the total power. The empirical cluster shadow fading distributions are unimodal with standard deviations ranging from 1.5 to 4.5 dB's. A lognormal model for cluster shadow fading appears to be a reasonable first choice, although more measurements should be evaluated for more reliable conclusions. The standard deviation of the composite signal is only about 1.5 dB, which is mostly explained by the small amount of measurement data.

To test the simplified cluster-based shadow fading model in Section III, we conducted the following experiment. We summed the shadow fading processes (obtained by sliding mean) of the strongest and the second strongest cluster. The histogram of the shadow fading power was then plotted. The procedure was repeated by cumulatively summing powers of all clusters so that the weakest cluster was summed last. The results for each step are shown in Fig. 8. We observe

[4]Sliding median processing gave the same results to within a small fraction of a dB [34].

that as the number of clusters increases the shadow fading distribution of the composite signal converges to a unimodal distribution resembling a Gaussian pdf. The shadow fading distribution of the original signal is shown for comparison in the lower subplot of Fig. 9. In the upper subplot of the same figure we show the reconstructed signal obtained by summing the shadow fading processes of the ten clusters. There is clear similarity with the shadow fading process of the original signal, although small differences can also be seen. The differences are explained by the limitations of the measurement system and data processing procedures. First, about 7.4% of the power of the original signal could not be clustered. The residual power, i.e., the error signal in Fig. 9, is attributed to short-time sporadic reflections and diffuse scattering. Second, due to limited dynamic range of the measurement system, weaker clusters often fade below the noise floor, in some cases reappearing at a later time instant. Therefore, the cluster power signals have many discontinuities, which complicates sliding window processing. Considering the many challenges in data processing, the results from measurement analysis are quite illuminating. In particular, Fig. 9 confirms that the shadow fading processes of individual clusters are the reason for the shadow fading of the composite signal. To make more general conclusions more measurement routes should be analyzed.

V. Discussion and Comparison to Literature

As we are presenting a new look to an old problem, it is important to compare our results to previous work. In this section we interpret, from the perspective of the new model, certain characteristics of shadow fading observed in literature. Implications to channel modelling will also be briefly discussed.

A. Local and Global Shadow Fading

It has been noticed by several investigators that the size of the analyzed geographical area has a strong influence on the standard deviation of shadow fading [35]–[38]. For measurement route lengths of $200 - 800$ meters in urban and rural environments standard deviations of $2.7 - 5.6$ dB are reported in the aforementioned references. This is clearly less than the values cited for measurement lengths of several kilometers, usually in the range of $6 - 12$ dB, see e.g. [1],

[39]–[44]. Based on the measurement evidence it makes sense to distinguish between shadow fading in local and global scale[5]. We can formalize the notions of local and global shadow fading by using the definitions of local area and extended local area from Section II. While such definitions cannot be unique, they can nevertheless provide guidelines for practical measurement data analysis.

Definition 3: We define *local shadow fading* as the variation of local area power within an extended local area. *Global shadow fading*, in turn, is defined as the variation of local area power over two or more extended local areas.

From Definition 3 it is clear, that the results in this paper apply mainly to local shadow fading, although the results can also partly explain the global shadow fading. The two types of shadow fading differ in underlying propagation mechanisms, measurement analysis, and utility. For sake of clarifying Definition 3 we shall briefly discuss these issues below.

1) Propagation Mechanisms: Local shadow fading is the variation of local area power within an extended local area. Result 1 states that local shadow fading may be caused by slow variations in plane wave powers. Other possible causes, not analyzed in this paper, may be interference between strong rays having small angular spacing (see comments in Section II-B), and short-term obstructions between the receiver and the last-bounce interacting objects.

In addition to local shadow fading[6], various other mechanisms including long-term obstructions due to buildings or hills, steep power transitions due to street corners, and random-like building heights [9], [10] contribute to global shadow fading. As the effect of these factors varies from an extended local area to another, it comes as no surprise that the standard deviation of global shadow fading is typically larger than that of local shadow fading.

2) Measurement Analysis: Local shadow fading can, in principle, be analyzed by dividing a continuous signal power measurement in segments whose dimensions correspond to extended

[5]In [35], terms ‘small area lognormal shadowing and ‘large area lognormal shadowing’ are used.

[6]The term local shadow fading is somewhat misplaced, since shadowing, or obstruction of a signal path, is probably not the main reason for variability in local area power within an extended local area. It should be noted, however, that an obstruction of plane waves (or clusters) does *not* violate the assumptions in Result 1 since the framework is probabilistic, and makes no assumptions on the underlying propagation mechanisms.

local areas. Large deterministic power transitions, e.g. due to movement from NLOS to LOS, should be removed from measurement data prior to analysis.

Analysis of global shadow fading involves processing long measurement lengths (i.e., several extended local areas) as a single set of data. Often global shadow fading is analyzed using curve fitting on a signal level measurement represented in a distance-path loss scatter plot. In other words, a path loss law, typically of form $A + m\log(d)$, with A constant and d the distance from the transmitter, is fitted to the measurement, and the residual error of the model fit is called shadow fading. Note that in this case the global shadow fading distribution will depend on the form of the path loss law and the fitting method, since, for a given data record, a dual-slope path loss model, for example, would surely result in a different shadow fading (i.e., residual error) distribution.

3) Utility: Simulation of local shadow fading is needed when path loss can be assumed constant over the simulation run. Typical usage includes evaluation of various link and system level algorithms. Simulation of global shadow fading, i.e., when simulation run spans over several extended local areas, is most commonly employed in network planning tools for signal level prediction purposes. As the fading standard deviations for the two cases are different, one should not use standard deviation obtained from a global shadow fading measurement analysis for simulation of local shadow fading, and vice versa.

B. Phenomena Explained from the Perspective of the New Model

Several phenomena reported in literature can be explained based on the model presented in this paper.

1) Small angular correlation: Consider a receiver that has two antennas with non-overlapping directional patterns. By measurements, it has been noted that the shadow fading correlation between the antenna branches is smaller than unity. A value of unity would be the expected value if all plane waves impinging at the receiver experienced the same multiplicative shadow fading process [45]. The observation that this is not the case fits into the framework presented in this paper in a very natural way. As was already conjectured in [12], [14], [45], the local shadow fading appears to be a phenomenon arising from the multipath phenomena. Therefore, from the viewpoint of the present model, local shadow fading is expected to be partly uncorrelated if the two receive antennas 'see' disjoint subsets of the N impinging plane waves, hence explaining the small angular correlation observed in measurements.

2) Distance independence: Standard deviation of shadow fading is usually reported being independent of the distance between transmitter and the receiver [35]–[37], [39], [46]–[48]. This observation can be explained in terms of the present model in which shadow fading is a result of local propagation phenomena near the receiver, and hence not affected by the intermediate propagation process taking place prior to the last-bounce interactions. This was also noted in [43], where results from several measurement campaigns were compared.

3) Correlation distance: Measurement studies indicate that the spatial 50% correlation distance of shadow fading is less than 10 meters for urban micro cells [36], [49], [50], $50-120$ meters for urban macro cells [35], [44], [51], and $50-400$ meters for suburban macro cells [35], [44], [49], [52]. In indoor cells, variations in average received power may occur even over the extent of an antenna array, i.e., for distances in the order of one meter [53]. In the additive model, correlation distance can be related to proximity of scatterers in the vicinity of the receiver. The rate of change of the angle of arrivals of the impinging plane waves as a function of travelled distance will then be faster than in macro cells, where the last-bounce scatterers are typically further away from the receiver than in micro and indoor cells. Variation in the angle of arrival translates to variation in the scattering cross-section of the last-bounce interacting object, which can be, for complex-shaped real-world objects, modelled as a random variable. As a result, the spatial correlation distances tend to be larger for environments where the interacting objects are not close to the receiver.

4) Non-Gaussian tails: As evident from the simulation results in Section IV, the additive model may produce skewed Gaussian-like distributions, depending on the ray power distributions. At first, this seems to be in contradiction with literature. A careful reading, however, reveals that a great majority of reported shadow fading distributions tend to be more or less skewed even for global shadow fading, which we hypothesize to be a result of even larger number of random factors than the local shadow fading analyzed in this paper. For examples, see e.g. [1, Figs. 2.37–2.40] [39, Figs. 36-37] [40, Figs. 9-12] [41, Figs. 2.4-1–2.4-4] [42, Fig. 4] [51, Fig.

7] [43, Fig. 5.33] [50, Fig. 1] [36, Fig. 7]. The literature review indicates that the shadow fading distribution in dB scale is Gaussian only near its mean value. Indeed, as has been pointed out at least in [36], [42], in simulations it is advisable to use truncated Gaussian distribution to avoid generation of samples from the tails of the Gaussian distribution, which often do not fit well the empirical distribution.

5) Rice-Lognormal Model: It has been proposed, for both satellite and land mobile communications systems, that variation in the power of the line-of-sight (LOS) signal component can be modelled with a lognormal distribution giving rise to the Rice-lognormal amplitude model [54], [55]. In LOS propagation, the first-arriving paths[7] carry most of the received signal power. A deterministic model based on interference of direct and reflected paths has also been proposed [12]. Interestingly, the lognormality of the first-arriving path can also be explained based on the additive model presented in this work. Assuming that signal power in the first delay bin is a result of summation of several incoherent rays, the model presented in Section II applies directly. The shadow fading then results from random variations in the amplitudes of these rays.

C. Implications for Channel Modelling

Result 1 and the measurement results in Section IV show that the shadow fading statistics can be induced directly by assigning each ray (or cluster) an individual shadow fading distribution; in principle, there is no need for an artificial multiplicative factor accounting for variations in the local mean power of the compound signal. Moreover, in a geometric channel model, multiplying the cluster signals with a common shadow fading process would result in fully correlated cluster large-scale fading. In contrast, the measurement results presented in Section IV indicate that clusters' shadow fading is not fully correlated[8]. Therefore, for realistic simulation each cluster should exhibit its own shadow fading characteristics. The additive sum-of-sinusoids based model may also lead to more parsimonious UWB channel models, as, in principle, there is no need for

[7] Depending on delay resolution, ground and wall reflected paths may arrive in the same delay bin as the direct line-of-sight path.

[8] A more thorough measurement analysis of cluster large-scale fading is beyond the scope of this paper and will be discussed in a separate paper.

separate shadow fading factors for rays, clusters and for the compound signal within an extended local area [56].

VI. Conclusion

We have presented an additive model as a physical basis for shadow fading in an area where path loss can be assumed constant. It was shown that under mild conditions on the statistics of the powers of the impinging plane waves, the shadow fading of the received signal will have approximately lognormal distribution. The theoretical justifications were supported by simulation results, hence verifying that the proposed additive model is capable of explaining the approximate lognormality of local shadow fading. A simplified cluster-based model was introduced as a special case of the general sum-of-sinusoids model. Novel measurement results demonstrated that summation of clusters' shadow fading can account for most of the variation in the local mean power. The additive model presented in this paper can also guide the way for design of more realistic channel models, where there is no need for an artificial multiplicative factor to account for variations in the local mean received power. The results of this paper also offer a partial answer for explaining the lognormality of shadow fading in a larger, global area, although more research effort is needed in this direction.

Acknowledgment

Advice and encouragement from prof. Ernst Bonek is gratefully acknowledged.

References

[1] R. Steele, Ed., *Mobile Radio Communications*. Pentech Press, 1991.

[2] J. J. Egli, "Radio propagation above 40 MC over irregular terrain," *Proc. IRE*, vol. 45, no. 10, pp. 1383–1391, Oct. 1957.

[3] A. J. Coulson, A. G. Williamson, and R. G. Vaughan, "A statistical basis for lognormal shadowing effects in multipath fading channels," *IEEE Trans. Commun.*, vol. 46, no. 4, pp. 494–502, Apr. 1998.

[4] G. K. Karagiannidis, N. C. Sagias, and P. Mathiopoulos, "The N*Nakagami fading channel model," in *Proc. Int. Symp. Wirel. Comm. Syst.*, Sept. 2005, pp. 185–189.

[5] L. Vuokko, P. Vainikainen, and J. Takada, "Clusters extracted from measured propagation channels in macrocellular environments," *IEEE Trans. Antennas Propagat.*, vol. 53, no. 12, pp. 4089–4098, Dec. 2005.

[6] K. Kalliola, H. Laitinen, P. Vainikainen, M. Toeltsch, J. Laurila, and E. Bonek, “3-D double-directional radio channel characterization for urban macrocellular applications,” *IEEE Trans. Antennas Propagat.*, vol. 51, no. 11, pp. 3122–3133, Nov. 2003.

[7] J. B. Andersen, “Statistical distributions in mobile communications using multiple scattering,” in *Proc. 27th URSI General Assembly*, Maastricht, Netherlands, Aug. 2002.

[8] A. Abdi and M. Kaveh, “On the utility of gamma pdf in modeling shadow fading (slow fading),” in *Proc. IEEE Veh. Tech. Conf.*, vol. 3, Houston, USA, May 1999, pp. 2308–2312.

[9] S. R. Saunders and F. Bonar, “Mobile radio propagation in built-up areas: a numerical model of slow fading,” in *Proc. IEEE 41st Veh. Tech. Conf.*, 1991, pp. 295–300.

[10] C. Chrysanthou and H. L. Bertoni, “Variability of sector averaged signals for UHF propagation in cities,” *IEEE Trans. Veh. Technol.*, vol. 39, no. 4, pp. 352–358, Nov. 1990.

[11] J. B. Andersen and I. Z. Kovács, “Power distributions revisited,” in *Proc. COST273 3rd Management Committee Meeting*, Jan. 17-18, 2002, Guildford, UK, TD(02)004.

[12] S. A. Abbas and A. U. Sheikh, “On understanding the nature of slow fading in LOS microcellular channels,” in *Proc. 47th IEEE Veh. Tech. Conf.*, vol. 2, 1997, pp. 662 – 666.

[13] G. D. Durgin, *Space-Time Wireless Channels*. Prentice-Hall, 2003.

[14] R. J. C. Bultitude, G. Brussaard, M. H. A. J. Herben, and T. J. Willink, “Radio channel modelling for terrestrial vehicular mobile applications,” in *Proc. Millen. Conf. Ant. Prop. (AP2000)*, Davos, Switzerland, Apr. 2000.

[15] G. L. Turin, F. D. Clapp, T. L. Johnston, S. B. Fine, and D. Lavry, “A statistical model of urban multipath propagation,” *IEEE Trans. Veh. Technol.*, vol. 21, no. 1, pp. 1–9, Feb. 1972.

[16] A. F. Molisch, J. R. Foerster, and M. Pendergrass, “Channel models for ultrawideband personal area networks,” *IEEE Wir. Comm.*, vol. 10, no. 6, pp. 14–21, Dec. 2003.

[17] S. S. Ghassemzadeh, R. Jana, C. W. Rice, W. Turin, and V. Tarokh, “Measurement and modeling of an ultra-wide bandwidth indoor channel,” *IEEE Trans. Commun.*, vol. 52, no. 10, pp. 1786–1796, Oct. 2004.

[18] J. Karedal, S. Wyne, P. Almers, F. Tufvesson, and A. F. Molisch, “Statistical analysis of the UWB channel in an industrial environment,” in *Proc. IEEE Veh. Tech. Conf.*, vol. 1, Los Angeles, USA, Sept. 2004, pp. 81–85.

[19] R. J.-M. Cramer, R. A. Scholtz, and M. Z. Win, “Evaluation of an ultra-wide-band propagation channel,” *IEEE Trans. Antennas Propagat.*, vol. 50, no. 5, pp. 561–570, May 2002.

[20] R. M. Buehrer, W. A. Davis, A. Safaai-Jazi, and D. Sweeney, “Characterization of the ultra-wideband channel,” in *Proc. IEEE Conf. Ultra Wideband Syst. Tech.*, Nov. 2003, pp. 26–31.

[21] P. Billingsley, *Probability And Measure*, 3rd ed. John Wiley & Sons, Inc., 1995.

[22] R. J. Serfling, *Approximation Theorems of Mathematical Statistics*. John Wiley & Sons, Inc., 1980.

[23] P. Billingsley, *Convergence of Probability Measures*, 2nd ed. John Wiley & Sons, Inc., 1999.

[24] Q. H. Spencer, B. D. Jeffs, M. A. Jensen, and A. L. Swindlehurst, “Measurement and modeling of temporal and spatial indoor multipath characteristics,” *IEEE J. Select. Areas Commun.*, vol. 18, no. 3, pp. 347–360, Mar. 2000.

[25] L. M. Correia, Ed., *Wireless Flexible Personalised Communications*. John Wiley, 2001.

[26] C.-C. Chong, C.-M. Tan, D. I. Laurenson, S. McLaughlin, M. A. Beach, and A. R. Nix, “A new statistical wideband

spatio-temporal channel model for 5-GHz band WLAN systems," *IEEE J. Select. Areas Commun.*, vol. 21, no. 2, pp. 139–150, Feb. 2003.

[27] L. Vuokko, P. Vainikainen, and J. Takada, "Clusterization of measured direction-of-arrival data in an urban macrocellular environment," in *Proc. PIMRC 2003*, vol. 2, Sept. 2003, pp. 1222–1226.

[28] N. Czink, M. Herdin, H. Özcelik, and E. Bonek, "Number of multipath clusters in indoor MIMO propagation environments," *El. Lett.*, vol. 40, no. 23, pp. 1498–1499, Nov. 2004.

[29] "Spatial channel model for Multiple Input Multiple Output (MIMO) simulations (3GPP TR 25.996), v6.1.0," Sept. 2003. [Online]. Available: www.3gpp.org

[30] A. F. Molisch, "A generic model for MIMO wireless propagation channels in macro- and microcells," *IEEE Trans. Signal Processing*, vol. 52, no. 1, pp. 61–71, Jan. 2004.

[31] G. C. Hess, *Handbook of Land-Mobile Radio System Coverage*. Artech House, Inc, 1997.

[32] A. Papoulis, *Probability, random variables, and stochastic processes*. McGraw-Hill, 1965.

[33] K. Kalliola, H. Laitinen, L. I. Vaskelainen, and P. Vainikainen, "Real-time 3-D spatial-temporal dual-polarized measurement of wideband radio channel at mobile station," *IEEE Trans. Instrum. Meas.*, vol. 49, no. 2, pp. 439–448, Apr. 2000.

[34] J. Salo, L. Vuokko, and P. Vainikainen, "Why is shadow fading lognormal?" in *Proc. International Symposium on Wireless Personal Multimedia Communications (WPMC'05)*, Aalborg, Denmark, Sept. 2005, pp. 522–526.

[35] M. J. Marsan, G. C. Hess, and S. S. Gilbert, "Shadowing variability in an urban land mobile environment at 900 MHz," *El. Lett.*, vol. 26, no. 10, pp. 646–648, May 1990.

[36] J.-E. Berg, R. Bownds, and F. Lotse, "Path loss and fading models for microcells at 900 MHz," in *Proc. IEEE Veh. Tech. Conf. (spring)*, vol. 2, Denver, USA, May 1992, pp. 666–671.

[37] S. Mockford, A. M. D. Turkmani, and J. D. Parsons, "Local mean signal variability in rural areas at 900 MHz," in *Proc. IEEE Veh. Tech. Conf. (spring)*, May 1990, pp. 610–615.

[38] K. Zayana and B. Guisnet, "Measurements and modelisation of shadowing cross-correlations between two base-stations," in *Proc. IEEE Int. Conf. Univ. Pers. Comm.*, vol. 1, Oct. 1998, pp. 101–105.

[39] Y. Okumura, T. Kawano, and K. Fukuda, "Field strength and its variability in VHF and land mobile radio service," *Rev. Elec. Commun. Lab.*, vol. 16, pp. 825–873, 1968.

[40] F. I. Meno, "Mobile radio fading in Scandinavian terrain," *IEEE Trans. Veh. Technol.*, vol. 26, no. 4, pp. 335–340, Nov. 1977.

[41] W. C. Jakes, Ed., *Microwave Mobile Communications*. IEEE Press, 1994.

[42] V. Erceg, L. J. Greenstein, S. Y. Tjandra, S. R. Parkoff, A. Gupta, B. Kulic, A. A. Julius, and R. Bianchi, "An empirically based path loss model for wireless channels in suburban environments," *IEEE J. Select. Areas Commun.*, vol. 17, no. 7, pp. 1205–1211, July 1999.

[43] D. Parsons, *The Mobile Radio Propagation Channel*. Halsted Press, 1992.

[44] A. Algans, K. I. Pedersen, and P. E. Mogensen, "Experimental analysis of joint statistical properties of azimuth spread, delay spread, and shadow fading," *IEEE J. Select. Areas Commun.*, vol. 20, no. 3, pp. 523–531, Apr. 2002.

[45] Wim A. Th. Kotterman, G. F. Pedersen, K. Olesen, and P. Eggers, "Correlation properties for radio channels from multiple base stations to two antennas on a small handheld terminal," in *Proc. IEEE 56th Veh. Tech. Conf.*, vol. 1, Sept. 2002, pp. 462 – 466.

[46] A. Mawira, “Models for the spatial correlation functions of the (log)-normal component of the variability of VHF/UHF field strength in urban environment,” in *Proc. IEEE Symp. Pers. Indoor Mob. Radio Comm.*, Oct. 1992, pp. 436–440.

[47] S. Kozono and K. Watanabe, “Influence of environmental buildings on UHF land mobile radio propagation,” *IEEE Trans. Commun.*, vol. 25, no. 10, pp. 1133–1143, Oct. 1977.

[48] S. R. Saunders, *Antennas and Propagation for Wireless Communication Systems*. John Wiley & Sons, Inc., 1999.

[49] M. Gudmundson, “Correlation model for shadow fading in mobile radio systems,” *El. Lett.*, vol. 27, no. 23, pp. 2145–2146, Nov. 1991.

[50] T. B. Sørensen, “Correlation model for slow fading in a small urban macro cell,” in *Proc. IEEE Int. Symp. Pers. Indoor Mob. Radio Comm. (PIMRC)*, vol. 3, Boston, USA, Sept. 1998, pp. 1161–1165.

[51] J. Weitzen and T. J. Lowe, “Measurement of angular and distance correlation properties of log-normal shadowing at 1900 MHz and its application to design of PCS systems,” *IEEE Trans. Veh. Technol.*, vol. 51, no. 2, pp. 265–273, Mar. 2002.

[52] E. Perahia, D. C. Cox, and S. Ho, “Shadow fading cross-correlation between base stations,” in *Proc. IEEE Veh. Tech. Conf. (spring)*, vol. 1, Rhodes, Greece, May 2001, pp. 313–317.

[53] H. Özcelik, “Indoor MIMO channel models,” Ph.D. dissertation, Technische Universität Wien, 2004.

[54] C. Loo, “A statistical model for land mobile satellite link,” *IEEE Trans. Veh. Technol.*, vol. 34, pp. 122–127, Aug. 1985.

[55] F. Vatalaro, “Generalised Rice-lognormal channel model for wireless communications,” *El. Lett.*, vol. 31, no. 22, pp. 1899–1900, Oct. 1995.

[56] *Channel Modelling Sub-Committee Report Final*, IEEE Std. IEEE802.15-02/490, 2002. [Online]. Available: http://ieee802.org/15/

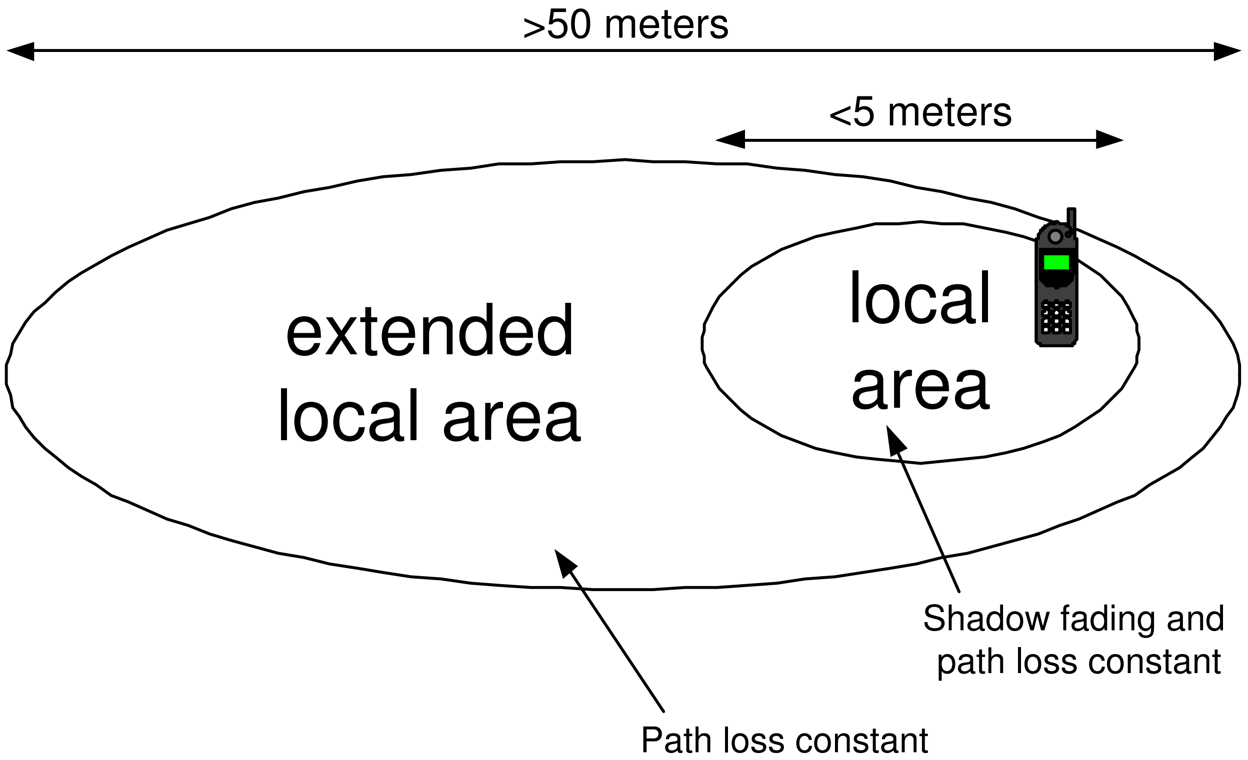

Fig. 1. Local area is defined as a region where path loss and shadow fading are constant. Extended local area, which consists of several overlapping local areas, is a region where only path loss is constant. The number of plane waves, N, is also assumed constant within the extended local area. The dimensions of the areas are indicative values based on measurements in an urban macro cell environment.

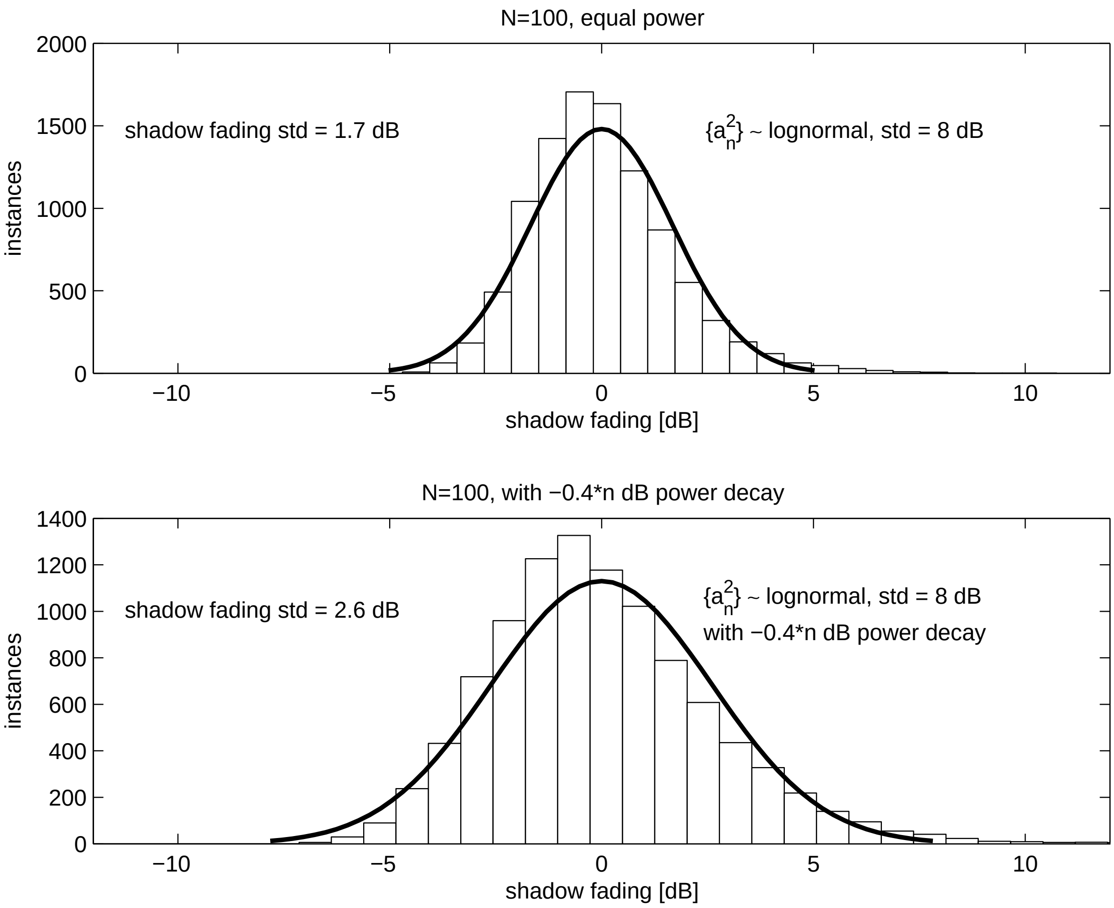

Fig. 2. Example of shadow fading distribution resulting from $N = 100$ plane waves. The x-axis shows $10 \log_{10}(\mathcal{P}_N)$. The plane wave powers are distributed as $\{b_n Y_n\}_{n=1}^N$, where $\{Y_n\}_{n=1}^N$ are iid lognormal random variables with zero-mean and 8 dB standard deviation. In the upper plot, $\{b_n\}_{n=1}^N = 1$. In the lower plot, $10 \log_{10}(b_n) = -0.4n$ dB, $n = 0, \ldots, 99$. The best-fit Gaussian is shown for reference.

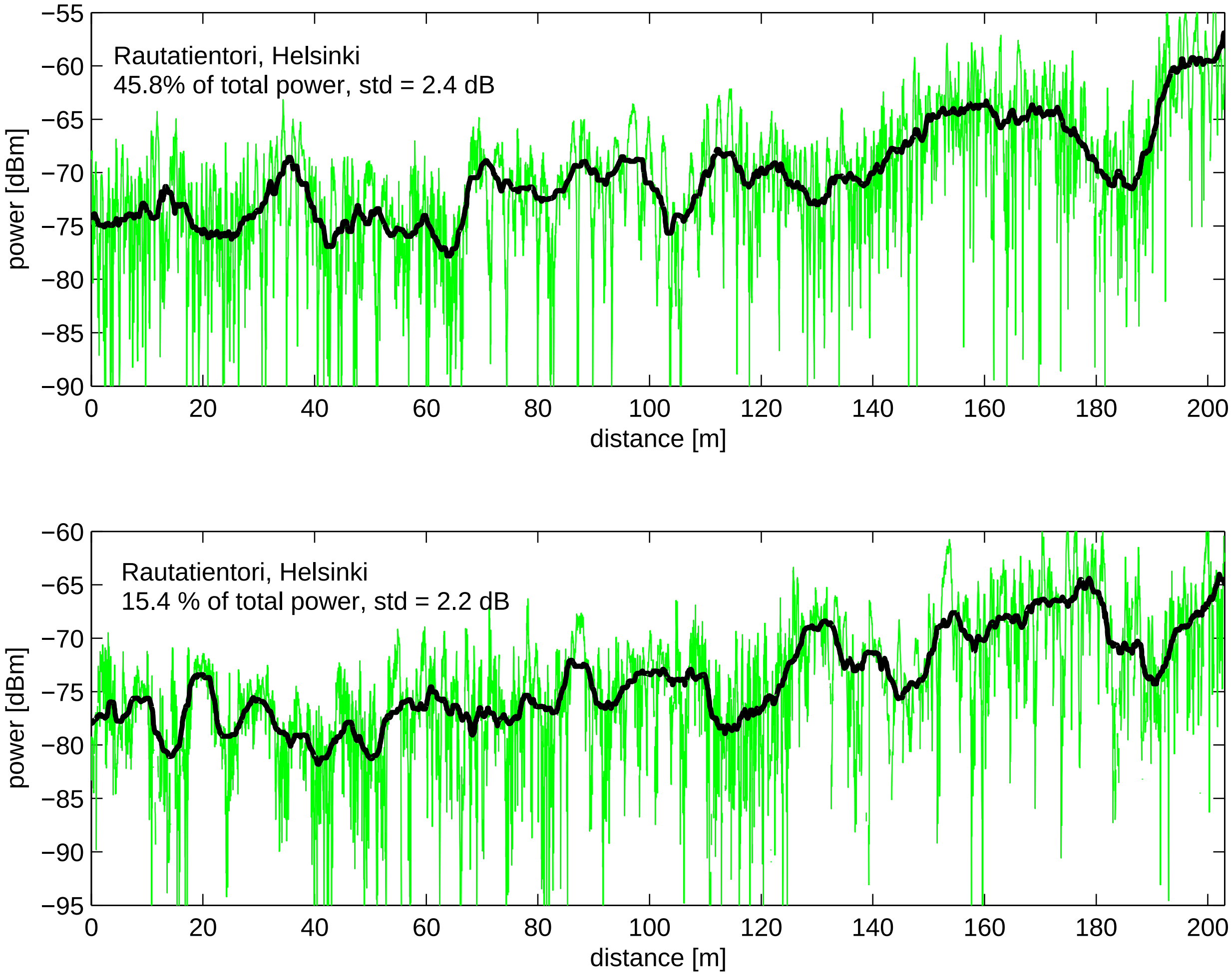

Fig. 3. Signals from two clusters extracted from an outdoor urban macrocell measurement [5]. In addition to small-scale fading, individual clusters exhibit also large-scale fading.

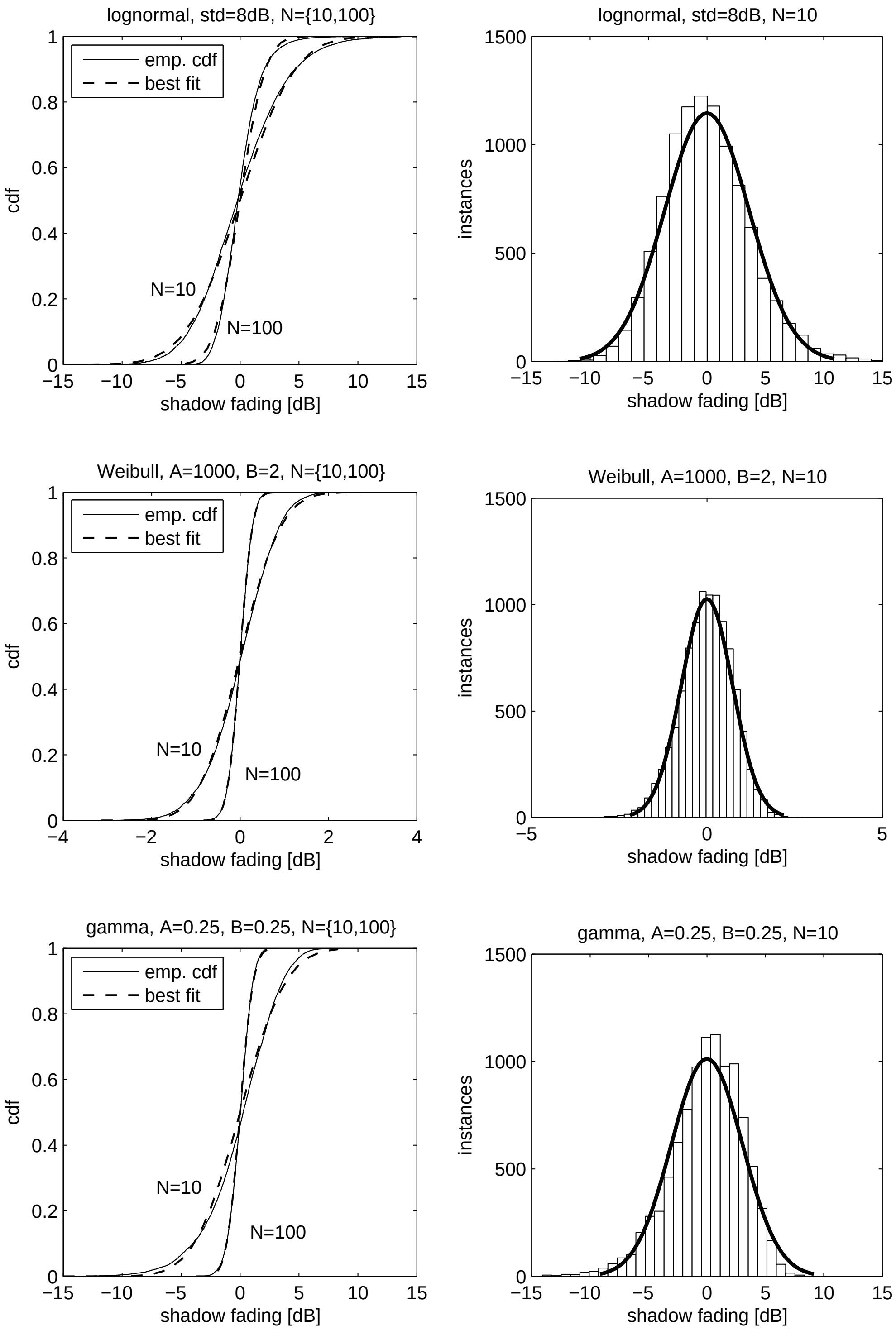

Fig. 4. Left: Empirical cdfs of $10\log_{10}(\mathcal{P}_N)$ resulting from different distributions for $\{\mathcal{A}_n^2\}_{n=1}^N$ for $N = \{10, 100\}$. Right: histogram for the case $N = 10$. In all cases the random variables $\{\mathcal{A}_n^2\}$ are iid. The gamma and Weibull pdfs are $f_X(x) = \frac{1}{B^A\Gamma(A)} x^{A-1} \exp\left(-\frac{x}{B}\right)$ and $f_X(x) = BA^{-B}x^{B-1}\exp\left[-\left(\frac{x}{A}\right)^B\right]$, respectively. The best-fit Gaussian distributions are also shown for comparison.

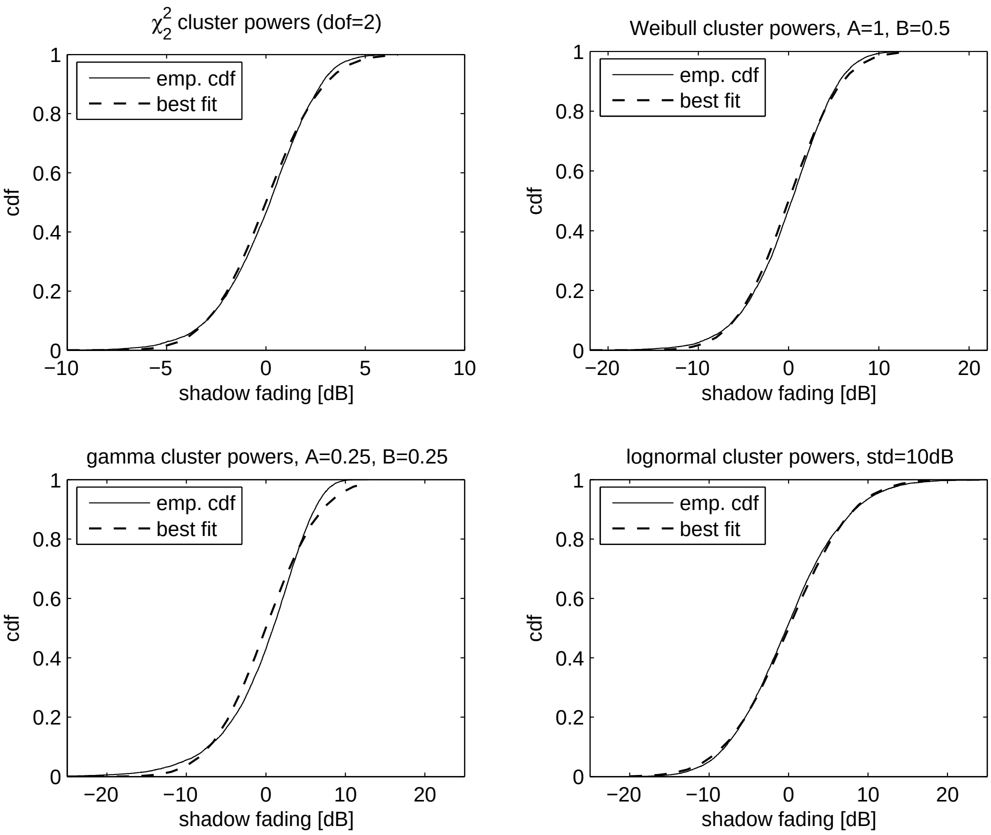

Fig. 5. Examples of shadow fading distributions resulting from different cluster power distributions. In all cases the number of clusters is four ($K = 4$), and the cluster powers $\{\mathcal{W}_k^2\}_{k=1}^{K}$ have iid pdfs. The best-fit Gaussian pdf is also shown for comparison.

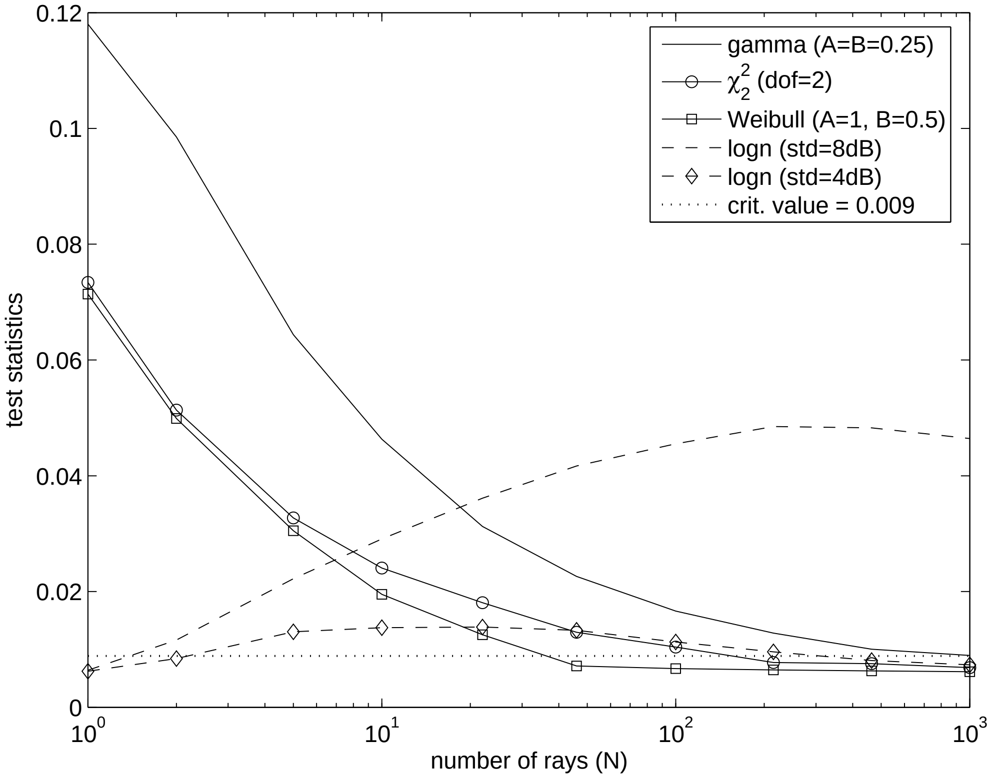

Fig. 6. Modified Kolmogorov-Smirnov hypothesis test to compare the goodness of fit of $10\log_{10}(\mathcal{P}_N)$ to Gaussian distribution. The critical value for 5% significance level is also shown. Small value of the test statistics indicates good fit.

TABLE I

SUMMARY OF MEASUREMENTS

Parameter	Value
Environment	Small urban macrocell, center of Helsinki
Carrier freq.	2.1 GHz
Tx / Rx antenna height	$25/1.5$ meters
Tx – Rx distance	≈ 300 meters
Meas. route length	≈ 200 meters
Estimation method	beamforming for each delay bin [33]

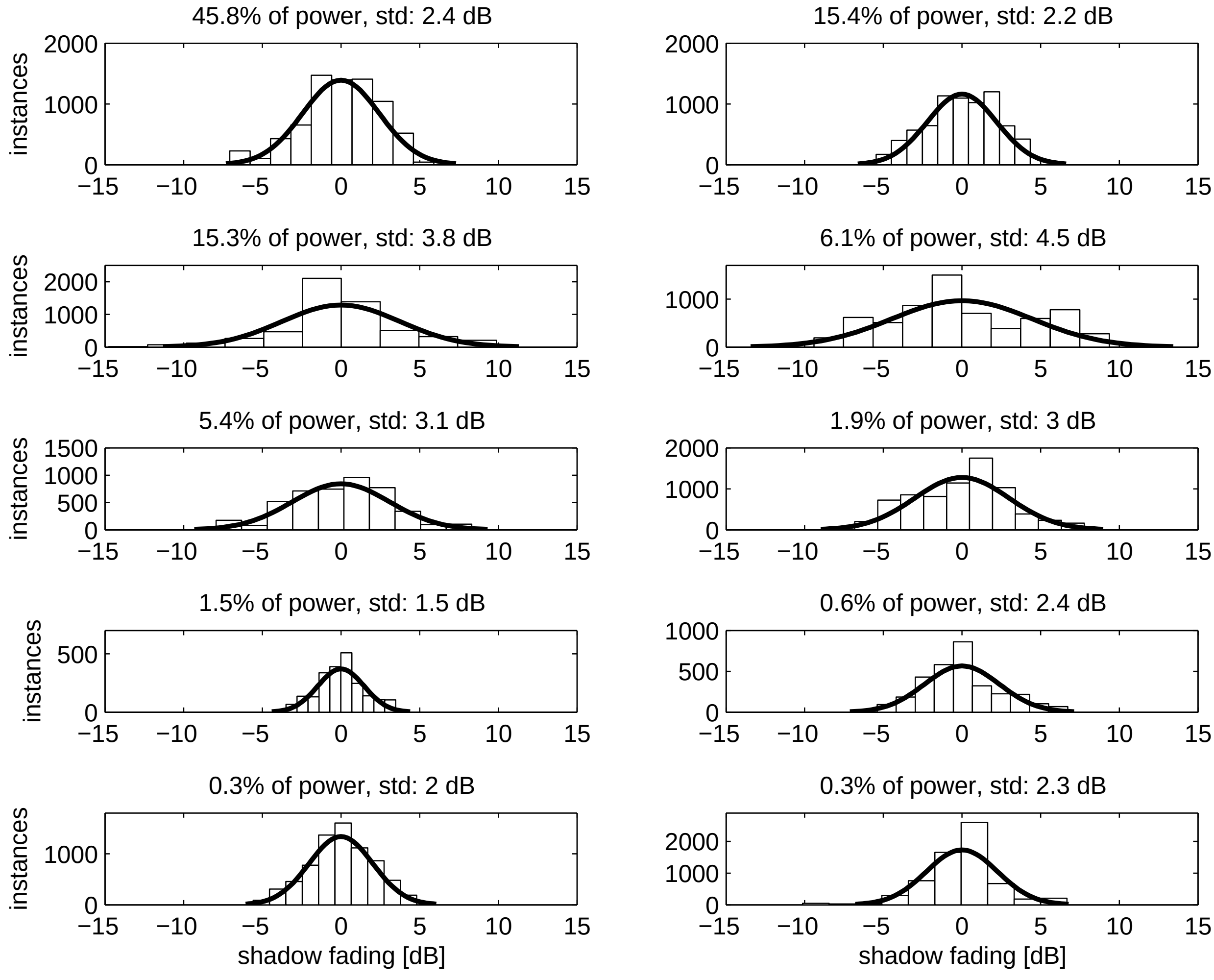

Fig. 7. Measured shadow fading histograms of the ten extracted clusters. The best-fit Gaussian pdf is also shown for comparison.

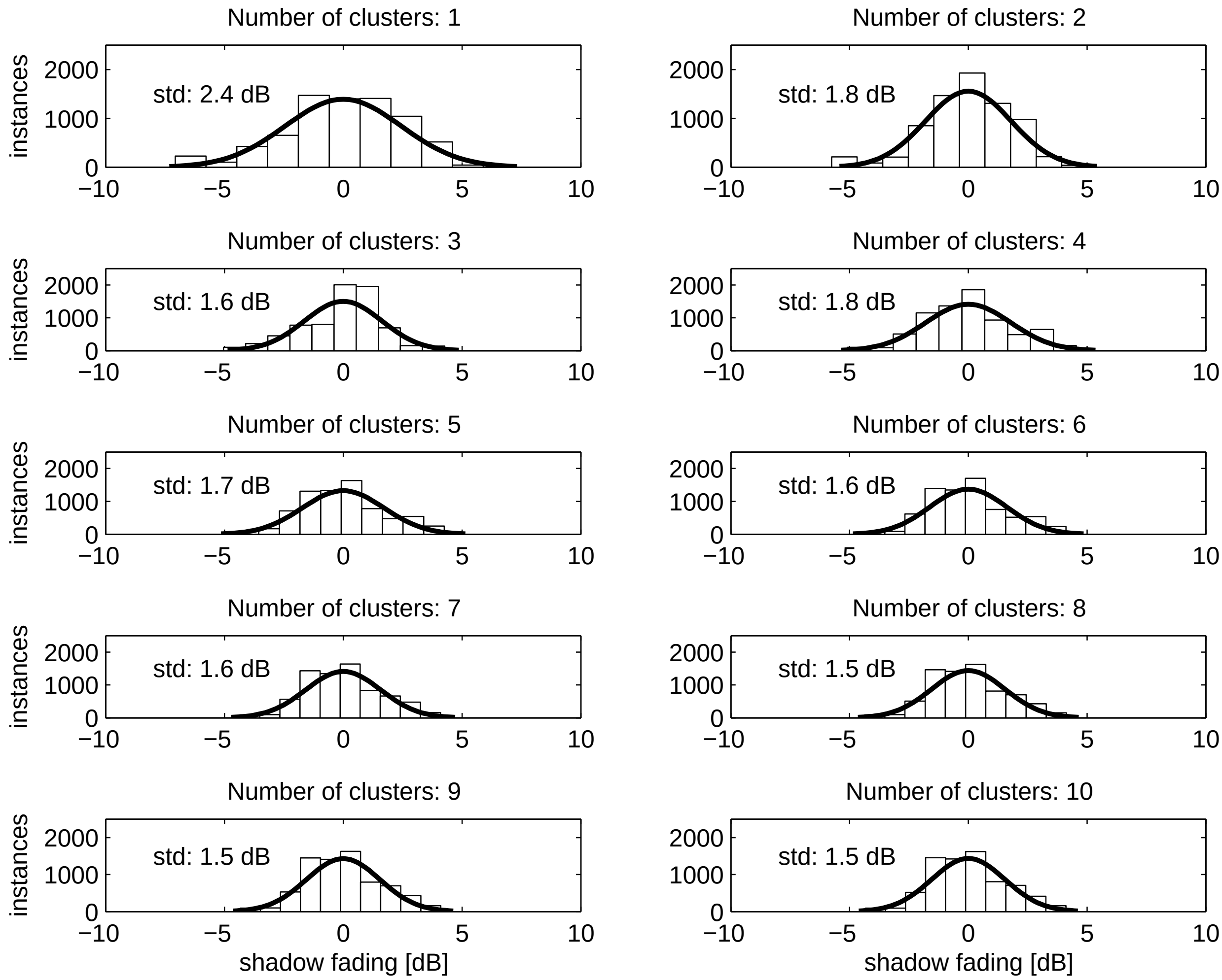

Fig. 8. Shadow fading histograms resulting from summing clusters' shadow fading signals one at the time. The best-fit Gaussian pdf is also shown for comparison.

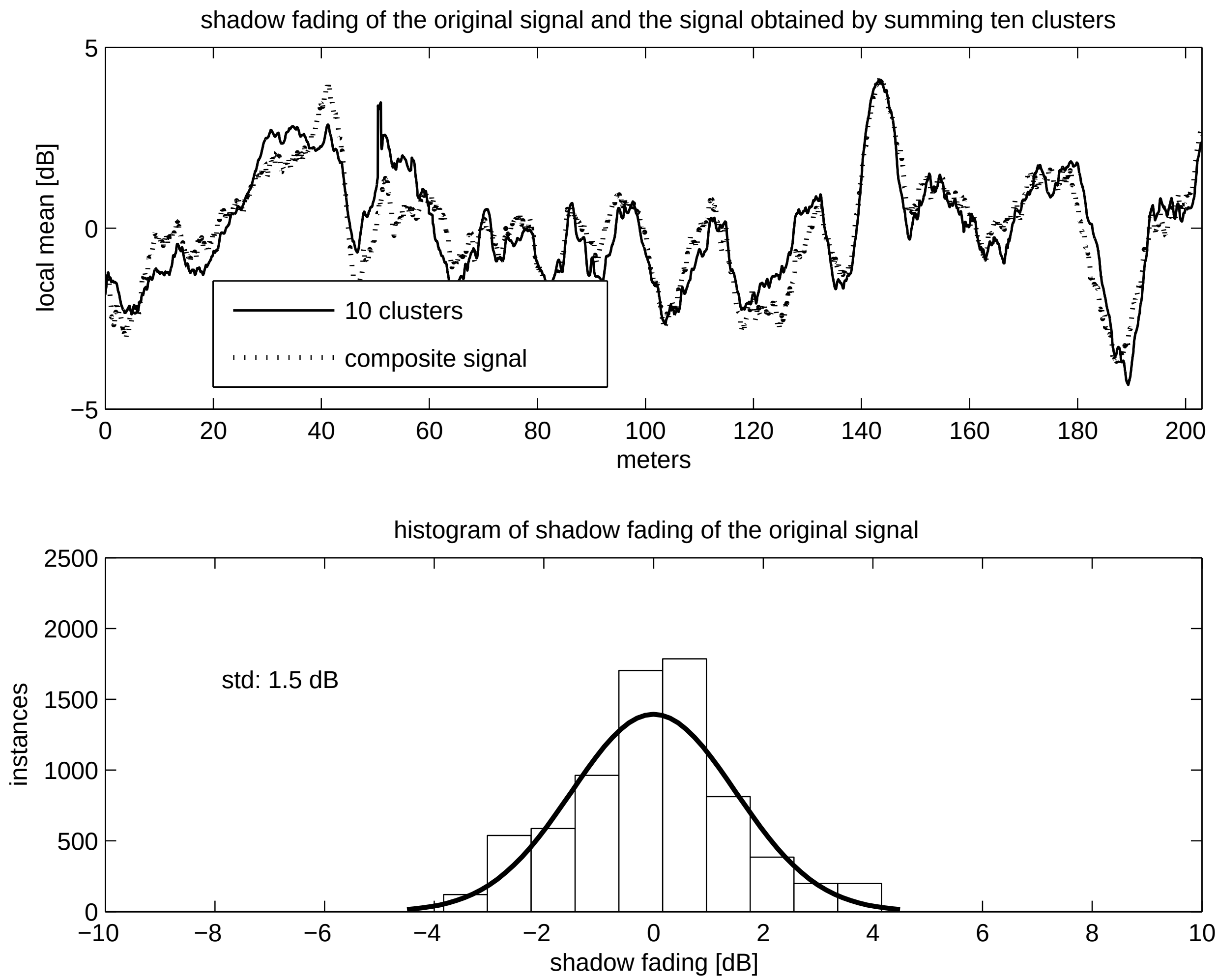

Fig. 9. Shadow fading process of the original measured signal, and signal reconstructed by summing the shadow fadings of ten clusters.